Regulation of Local Structure and Composition of Binary Disulfide and Thiol Self-Assembled Monolayers Using Nanografting

Donglei Bu,[†] Thomas J. Mullen,[†,‡] and Gang-yu Liu[†,‡,*]

[†]Department of Chemistry and [‡]Nanomaterials in the Environment, Agriculture and Technology, Organized Research Unit, University of California, Davis, California 95616, United States

ABSTRACT Nanografting is used to create spatial confinement, which enables regulation of self-assembly reaction pathways and outcome. The degree and outcome of this regulation is revealed using binary self-assembled monolayers (SAMs) of organothiols and disulfides. In naturally grown systems, these SAMs have more complex morphology when compared with corresponding binary alkanethiol SAMs. Taller molecules form nanodomains of ellipsoidal cap in shape. These domains arrange in various irregular geometries, including 1D worm-like and 2D branches. This observation differs from binary alkanethiol SAMs, where nanodomains are separated and randomly dispersed. During nanografting, more homogeneous morphology was observed compared with naturally grown layers. By varying nanoshaving speed, the nanodomain structure can be regulated from randomly dispersed to more heterogeneous and, finally, to near natural growth. This trend is very similar to mixed alkanethiol systems, where the domain size and separation increase with increasing speed. Different from the alkanethiol systems, the observed structural variations are due to the changes in surface composition, in addition to domain size, shape, and arrangement.

KEYWORDS: self-assembled monolayer · nanografting · dialkyl disulfide · alkanethiol · surface concentration · lateral heterogeneity · spatial confinement

Multicomponent self-assembled monolayers (SAMs) of alkanethiols on noble metal surfaces are of great interest due to their rich surface structures and various terminal functionalities.[1,2] These mixed SAMs provide a platform to study and to regulate interfacial phenomena, such as wettability,[3] electron transfer,[4] biomaterial adhesion,[5−7] and molecular recognition.[8,9] Previous studies have shown that the physical and chemical properties of binary SAMs such as friction,[10] elastic compliance,[11] mechanical response,[12] and protein immobilization ability[13] are dependent on local lateral heterogeneity and/or surface composition. For example, the protein−surface interactions at the molecular level can be regulated by changing the binding domains and their local environment because the specific recognition sites are at the nanometer scale.[14] Therefore, an effective method to regulate the surface properties in terms of lateral heterogeneity and composition at the nanometer scale is critical to obtain the desired surface properties.

Dialkyl disulfide molecules are important precursors to the formation of SAMs because they are typically easier to synthesize and to preserve than their alkanethiol counterparts.[15,16] Further, dialkyl disulfide molecules with various reactive termini,[16] such as aldehyde[17,18] and biotin,[19] have been synthesized and made available. Single-component dialkyl disulfide and alkanethiol molecules form SAMs with indistinguishable physical and chemical properties on Au surfaces.[16,20] The lattice structures of dialkyl disulfide and alkanethiol SAMs on Au(111) yield hexagonal overlayers with a $c(\sqrt{3} \times \sqrt{3})R30°$ structure.[21] Heterodialkyl disulfide molecules form SAMs different from mixed binary thiols and thus are frequently used to generate molecular mixing.[22] Mixed SAMs formed from multicomponents of disulfide and alkanethiol molecules have not been investigated systematically. This work will reveal the structural complexity and introduce a means (*i.e.*, nanografting) to regulate their local structure. The structural characterization and structural and surface composition regulation of these classes of mixed SAMs will be compared with alkanethiol binary SAMs.[23] This investigation is of generic importance in enhancing our knowledge of local structures of mixed SAMs containing disulfide molecules, and the regulation of local structure is important to surface chemical and biological properties, such as protein immobilization.[24,25]

*Address correspondence to liu@chem.ucdavis.edu.

Received for review July 18, 2010 and accepted September 29, 2010.

Published online October 8, 2010.
10.1021/nn101680h

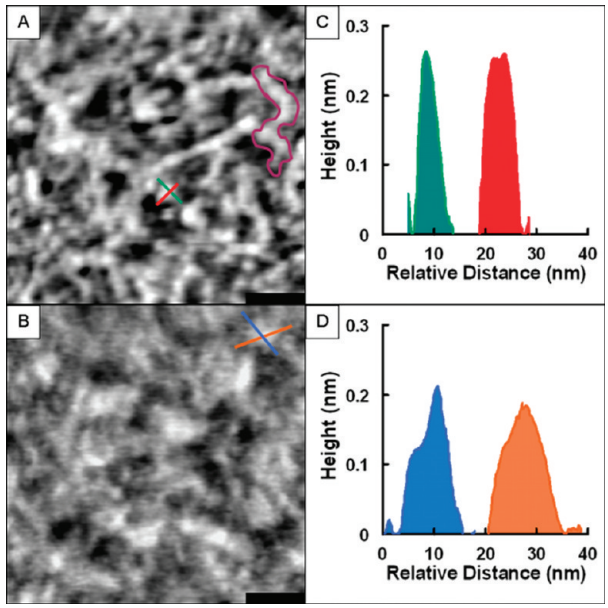

Figure 1. Comparison of the local structure of a naturally grown binary SAM formed from a 0.02 mM solution of SSC_{11}:SC_{18} = 5:3 and from a 0.02 mM solution of SC_{10}:SC_{18} = 5:3. (A) High-resolution AFM topograph of the SSC_{11}/SC_{18} SAM. The purple enclosure highlights a worm-like assembly of C_{18} domains. (B) High-resolution AFM topograph of the SC_{10}/SC_{18} binary SAM. (C,D) Corresponding cursor profiles as indicated in (A) and (B), respectively. Scale bars = 20 nm.

RESULTS AND DISCUSSION

High-Resolution Imaging of Binary SAMs of a Dialkyl Disulfide and an Alkanethiol. Naturally grown dialkyl disulfide:alkanethiol binary SAMs exhibit a more complex structure in terms of domain geometry and arrangement when compared to naturally grown binary alkanethiol SAMs. Figure 1A shows a high-resolution AFM topographic image of a naturally grown diundecyl disulfide (SSC_{11}):octadecanethiol (SC_{18}) binary SAM, while Figure 1B shows its counterpart: a decanethiol (SC_{10}):SC_{18} binary SAM. Both of these SAMs consist of segregated domains at the nanometer scale, which appear as bright, gray, and dark features. The dark regions include etch pits because their vertical depth (0.24 nm) equals the single atomic step height of Au(111), and their morphologies and distributions are consistent with previous scanning tunneling microscopy (STM) and AFM studies of single-component SAMs.[26−28]

For the SSC_{11}:SC_{18} binary SAM (Figure 1A), the ellipsoidal capped contrast shows domains of SC_{18} molecules, with average lateral dimensions of 5.6 nm (ranging from 4.0 to 7.2 nm) and 4.4 nm (ranging from 2.8 to 6.1 nm) along the long and short axes, respectively. These individual domains tend to group in line, following 1D worm-like or in 2D irregular branched arrangement. An example of this type of aggregate is highlighted by the purple enclosure in Figure 1A. In contrast, most of the SC_{18} domains within the SC_{10}:SC_{18} binary SAM (Figure 1B) are semi-ellipsoidal with larger average lateral dimensions of 10.3 nm (ranging from 7.0 to 15.0 nm) for the long axis and 7.8 nm (ranging from 4.8 to 12.2 nm) for the short axis. These SC_{18} domains appear to be more randomly dispersed and isolated when compared to the domains of the dialkyl disulfide:alkanethiol binary SAMs. To provide concrete measurements, Figure 1C shows a typical SC_{18} domain in the SSC_{11}:SC_{18} binary SAM, measuring 5.2 nm × 4.2 nm laterally. Using a typical worm-shaped assembly as selected in the purple enclosure, seven individual domains are posited side-by-side into a length of 51.0 nm. As a comparison, Figure 1D shows a typical SC_{18} domain in the SC_{10}:SC_{18} binary SAM, with 10.0 nm × 4.0 nm for the long and short axes, respectively. Compared with the separated and randomly dispersed domains in SC_{10}:SC_{18} binary SAMs, the domain structures in the SSC_{11}:SC_{18} binary is richer and more complex. Various irregular shaped (*e.g.*, worm-like shape) domain assemblies are commonly observed in the SSC_{11}:SC_{18} binary SAMs.

Nanografted Dialkyl Disulfide:Alkanethiol Binary SAMs Exhibit More Homogeneous Structure than the Naturally Grown Counterparts. Dialkyl disulfide:alkanethiol binary SAMs produced by nanografting exhibit a more homogeneous morphology when compared to their naturally grown counterparts. Figure 2A shows a naturally grown SSC_{11}:SC_{18} binary SAM with a nanografted region in the center. The boundaries are visible because the pattern is smoother and taller than the surrounding SAM. The origins of the height difference and its implications related to surface composition will be discussed in a later section. The smooth contrast is a clear indication that the nanografted regions are more homogeneous. This trend is further supported by high-resolution imaging of the local structure upon zooming into the two regions, as shown in Figure 2B and C, which correspond to naturally grown and nanografted regions of the SSC_{11}:SC_{18} binary SAM, respectively. The bright domains are mostly composed of the taller SC_{18} molecules; the gray domains are mostly composed of the shorter SSC_{11} molecules, and many of the dark features are due to etch pits and defects.

As discussed in the previous section, one origin of heterogeneity in natural growth is the arrangement of SC_{18} domains into lines and branches, such as the domain group highlighted by the purple enclosure in Figure 2B. In the nanografted region, most domains remain as individual. The size of individual SC_{18} domains may be quantified from topographic images, as illustrated by the cursor profiles in Figure 2D. In the naturally grown region, the selected SC_{18} domain has the lateral dimensions of 5.4 nm for the long axis and 4.5 nm for the short axis. This is comparable with the lateral dimensions of the SC_{18} domain in the nanografted region highlighted by the cursor profiles in Figure 2E, which has the lateral dimensions of 5.8 nm for the long axis and 4.9 nm for the short axis. Among the SC_{18} domains measured in both regions, the size of individual

domains is similar: the naturally grown SC_{18} domains have average lateral dimensions of 5.6 nm (4.0 to 7.2 nm) for the long axis and 4.4 nm (2.8 to 6.1 nm) for the short axis. The lateral dimensions in the nanografted region are 6.1 nm (4.3 to 7.7 nm) for the long axis and 4.8 nm (3.9 to 6.0 nm) for the short axis. Therefore, we conclude that the lateral heterogeneity of these binary SAMs is mainly due to the preferable grouping or arrangement of the SC_{18} domains.

Nanografting Enables Regulation of the Lateral Heterogeneity of Dialkyl Disulfide:Alkanethiol Binary SAMs. The lateral heterogeneity can be visualized and quantified from high-resolution AFM images. Figure 3A−C shows naturally grown and nanografted regions of SSC_{11}:SC_{18} binary SAMs produced at three nanoshaving speeds of 500, 3000, and 10 000 nm/s, respectively. The nanografted boundaries are visible because the patterned regions appear smoother and are taller than the surrounding naturally grown region. Figure 3D−F displays high-resolution AFM topographs by zooming into the nanografted regions at the three speeds, respectively. The bright domains are mostly composed of the taller SC_{18} molecules, and the gray domains are mostly composed of the shorter SSC_{11} molecules.

The SC_{18} domains are clearly visible at all three nanoshaving speeds. The size of these individual domains slightly decreases as the nanoshaving speed is increased. For example, the average lateral dimensions for the long × short axis of the SC_{18} domains in the nanografted regions decrease slightly from 6.1 nm × 4.8 nm at 500 nm/s to 5.3 nm × 3.9 nm at 10 000 nm/s. This small decrease in domain size is also illustrated in Figure 3G−I, where cursor profiles display the lateral dimensions and vertical heights of typical SC_{18} domains at the nanoshaving speeds of 500, 3000, and 10 000 nm/s, respectively.

A more pronounced change was observed in the arrangement of domains, that is, the preferred grouping of SC_{18} domains as the nanoshaving speed increases. At fast nanoshaving speeds, the structure and shape of these assemblies exhibit similarities to naturally grown SSC_{11}:SC_{18} binary SAMs (Figures 1A and 2B). As discussed in the previous section, domains appear evenly dispersed at a nanoshaving speed of 500 nm/s. At 3000 nm/s, complex and irregular-shaped domain assemblies begin to appear as highlighted by the purple enclosure in Figure 3E. This aggregate is composed of four individual domain units and is 17.2 nm in length. At 10 000 nm/s, larger worm-like and other irregular-shaped domain arrangements were observed. One example of a 43.4 nm long 1D assembly, defined by the purple frame, consists of eight individual domain units. The domain structures at 10 000 nm/s are most similar in geometry and lateral heterogeneity to the domain structures formed in the naturally grown SSC_{11}:SC_{18} binary SAM (Figures 1A and 2B).

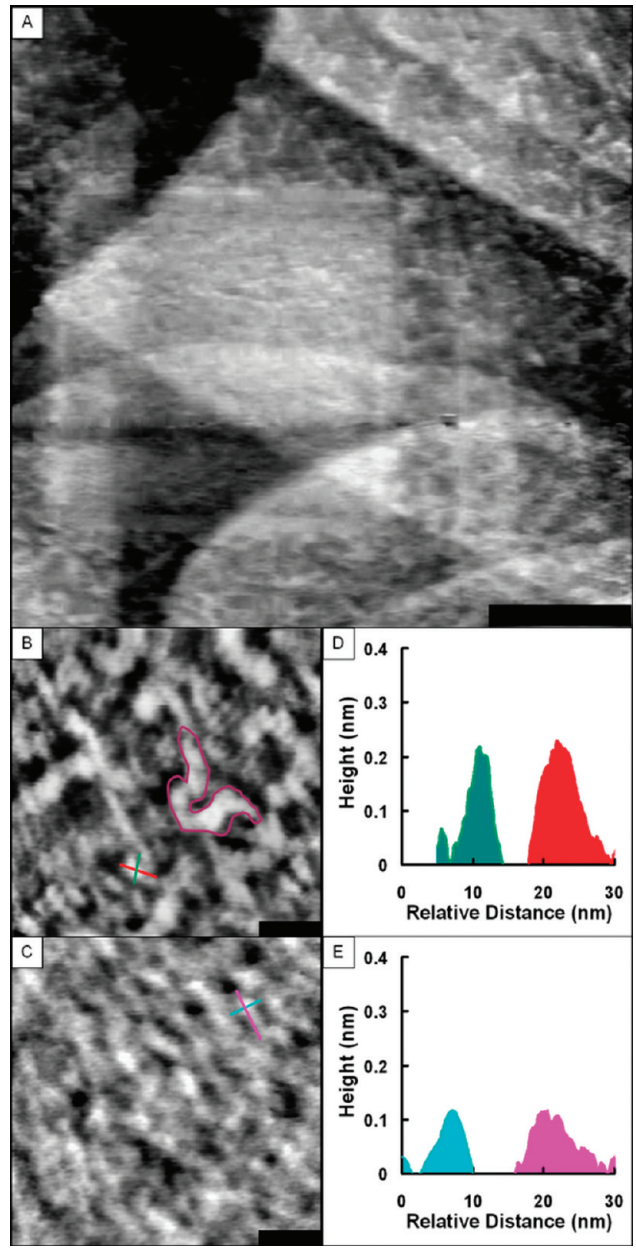

Figure 2. Comparison of local structure of the naturally grown and nanografted SAMs of a SSC_{11}:SC_{18}. The nanoshaving speed was 500 nm/s under the same 0.02 mM solution of SSC_{11}:SC_{18} = 5:3. (A) AFM topograph reveals the morphology of SAMs produced in the naturally grown and nanografted regions. Scale bar = 100 nm. (B) High-resolution AFM image of a naturally grown region from (A). The purple enclosure highlights a worm-like arrangement of C_{18} domains. (C) High-resolution image of a nanografted region from (A). (D,E) Corresponding cursor profiles as indicated in (B) and (C), respectively. Scale bars in (B) and (C) = 20 nm.

By changing the termini of the disulfide molecules from methyl to aldehyde moieties, the effects of the terminal group are investigated. Figure 4A−C shows naturally grown and nanografted regions of 11-mercapto-1-undecanal disulfide ($SSC_{10}CHO$):SC_{18} binary SAMs produced at three nanoshaving speeds, 500, 3000, and 10 000 nm/s, respectively. Figure 4D shows a naturally grown region of a $SSC_{10}CHO$:SC_{18} binary SAM. The nanografted boundaries are visible because the pat-

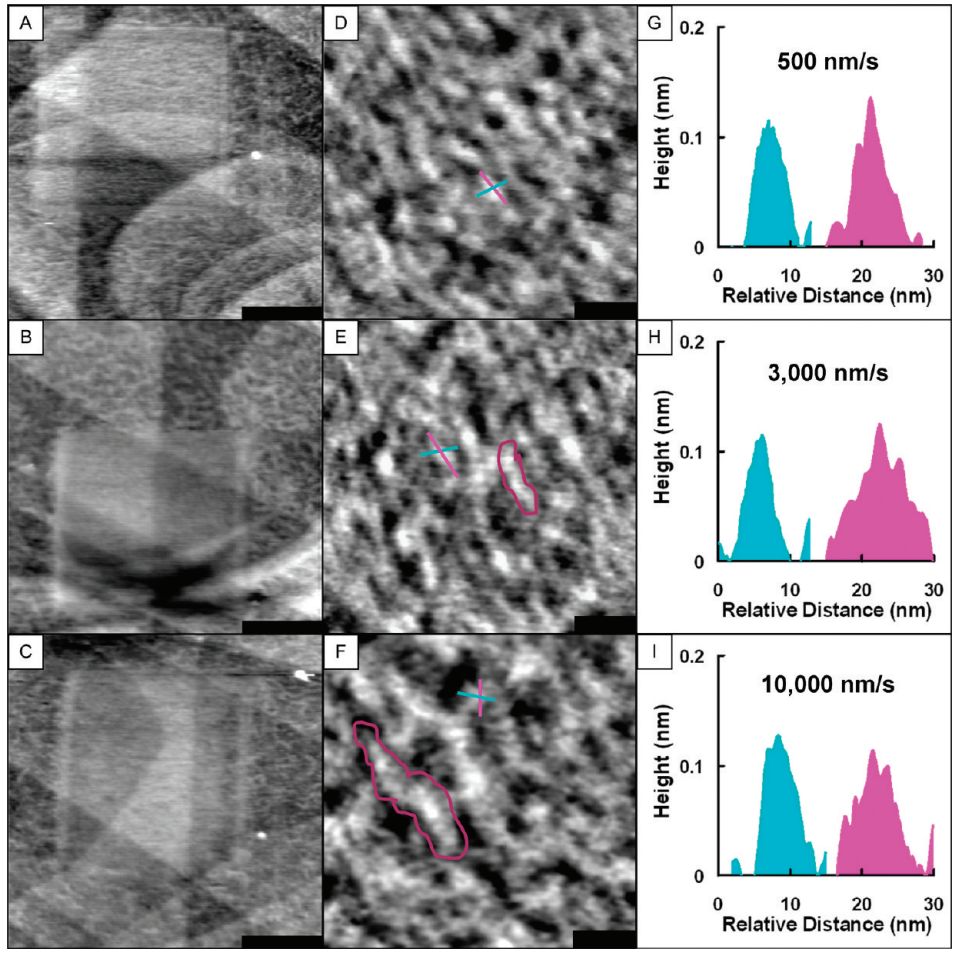

Figure 3. Comparison of the local structures of SSC_{11}:SC_{18} binary SAMs fabricated at three nanoshaving speeds: 500, 3000, and 10 000 nm/s, from top to bottom. Images (A−C) show an overview of the nanografted areas surrounded by the naturally grown matrix. (D−F) Zoom-in scans over the nanografted areas in (A−C), respectively. The purple enclosures highlight typical domain arrangements. (G−I) Corresponding cursor profiles as indicated in (D−F), respectively. Scale bars for the left column = 100 nm, and the scale bars for the middle column = 20 nm.

terned regions appear smoother and are taller than the surrounding naturally grown region. The origins of this height difference and its implications related to surface coverage will be discussed in a subsequent section. Figure 4E−G displays high-resolution AFM topographic images corresponding to the nanografted regions in Figure 4A−C, respectively. The size and distribution of these bright domains (*i.e.*, taller SC_{18} molecules) are clearly visible from those high-resolution views.

Consistent with SSC_{11}:SC_{18} binary SAMs, the $SSC_{10}CHO$:SC_{18} systems also exhibit SC_{18} domains at all three nanoshaving speeds and in the naturally grown SAMs. Figure 4I−L shows cursor profiles across characteristic SC_{18} domains, as indicated in Figure 4E−H, respectively. As the shaving speed increases from 500, 3000, to 10 000 nm/s, the size of SC_{18} domains increases and approaches the domain size of naturally grown SAMs. For example, the average lateral dimensions for the long axis (and short axis) of the SC_{18} domains decrease from 7.3 nm (5.1 nm) for the naturally grown region to 4.6 nm (3.7 nm) for the 500 nm/s nanografted region. As the nanoshaving speed is increased from 500 to 10 000 nm/s, the lateral dimensions for the long axis (and short axis) of the SC_{18} domains slightly increase to 6.9 nm (5.0 nm) at the nanoshaving speed of 10 000 nm/s. This approaches the lateral dimensions of the domains of the natural growth binary SAM. This trend differs from that in the SSC_{11}:SC_{18} binary SAMs, where a slight decrease in SC_{18} domain size occurred. A possible explanation is that the aldehyde moiety tends to cluster, in contrast to the alkanethiol binary SAMs with methyl termini.[23,29−32]

In addition to the change in lateral dimensions, irregular assemblies form and increase in size as the nanoshaving speed is increased for the $SSC_{10}CHO$:SC_{18} binary SAMs; this trend is consistent with the SSC_{11}:SC_{18} binary SAMs. At 500 nm/s, the surface is dominated by individual and dispersed domains. With the increasing nanoshaving speed, complex arrangements of these SC_{18} domains appear. At 3000 nm/s, linear grouping into worm-like arrangement was observed, as shown

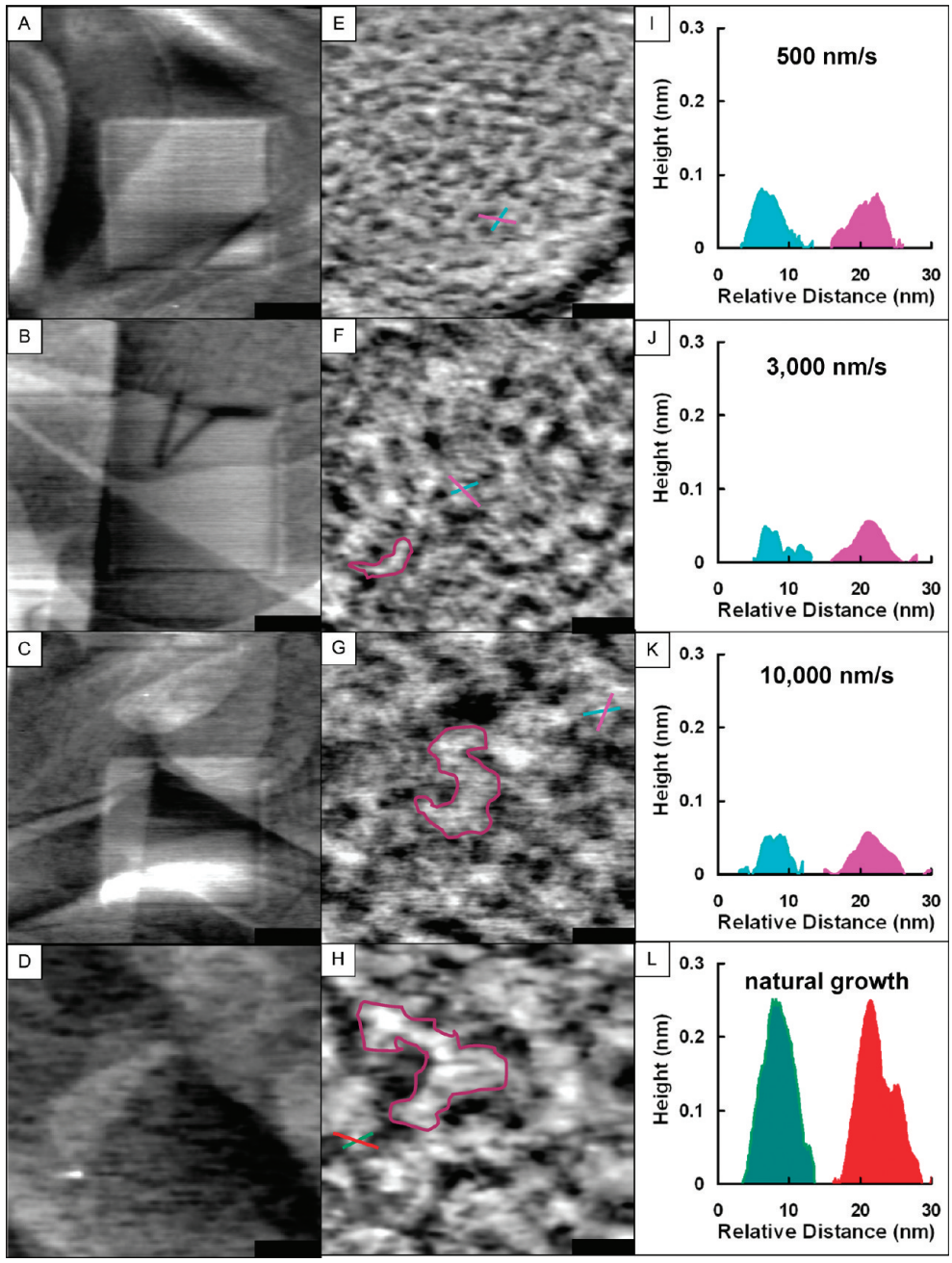

Figure 4. Comparison of the local structure of $SSC_{10}CHO:SC_{18}$ binary SAMs formed at three nanoshaving speeds, from top to bottom, 500, 3000, and 10 000 nm/s, and natural growth. AFM images in (A−C) show the overall topograph of the binary SAMs formed *via* nanografting and their surrounding of naturally grown matrix. (D) $SSC_{10}CHO:SC_{18}$ SAM formed by natural growth. (E−G) Zoom-in scans of the nanografted areas in (A−C), respectively. (H) Zoom-in image of (D). The purple frames highlight the typical arrangements of SC_{18} domains. (I−L) Corresponding cursor profiles as indicated in (E−H), respectively. Scale bars in the left column = 100 nm; scale bars in the middle column = 20 nm.

by the example inside the purple frame in Figure 4F: a 13.6 nm curve containing four domain units. At 10 000 nm/s, large irregular arrangements appeared. In the example defined by the purple enclosure in Figure 4G, nine SC_{18} domains follow a curve of 60.7 nm long. Similar to the methyl-terminated dialkyl disulfide:alkanethiol binary SAMs, the domains of the $SSC_{10}CHO:SC_{18}$ binary SAM nanografted at 10 000 nm/s resemble the geometry of the naturally grown SAMs. Generally, the SC_{18} domains of the $SSC_{10}CHO:SC_{18}$ binary SAMs are typically larger than that of the SC_{18} domains in $SSC_{11}:SC_{18}$ SAMs. We attribute this to a stronger terminal−terminal interaction (6 kcal/mol)[33] for the aldehyde groups when compared to the methyl functional groups (2 kcal/mol). The formation of aldehyde-terminated SAMs with higher segregation is consistent with previous reports on mixed alkanethiol SAMs with different termini.[23,29−32]

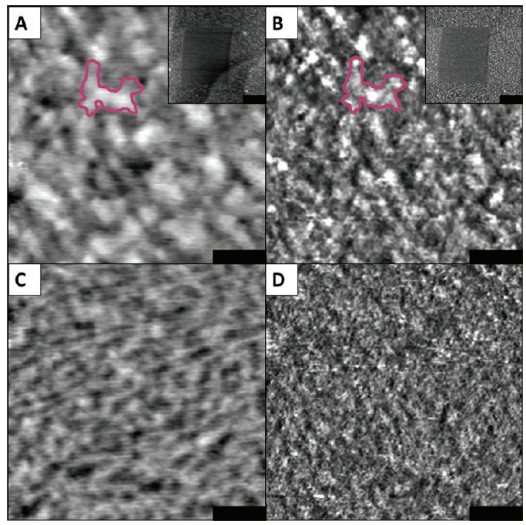

Figure 5. Comparison of surface structure of $SSC_{10}CHO$:SC_6 SAMs prepared by naturally growing and nanografting. (A,B) Topograph and simultaneous frictional force images from the naturally grown region. (C,D) Topograph and simultaneous frictional force images from the nanografted region. The overall morphology including the nanografted area and surrounding matrix is shown as the insets. Scale bars = 20 nm for images (A−D), and scale bars in the insets = 100 nm.

The observed regulation of heterogeneity by nanografting is robust, as also demonstrated in Figure 5, where naturally grown and nanografted $SSC_{10}CHO$: hexanethiol (SC_6) SAMs are compared *via* an AFM topograph and simultaneous lateral force images. The bright segregated features in Figure 5A represent the $SC_{10}CHO$ domains. This assignment is well-supported by the corresponding bright contrast in Figure 5B, indicating higher frictional force in these hydrophilic areas than the surrounding mainly with C_6 molecules. Typically, lateral force contrast is sharper than the topograph,[34−38] which facilitates our determination of $SSC_{10}CHO$ domain boundaries, as exampled in an irregular-shaped domain defined by the purple enclosure. This accurate determination of domain boundaries is an important step in extracting surface concentrations of each component (see later sections). In the nanografted regions, as shown in Figure 5C and D, the grain size appears much smaller than in Figure 5A and B, which indicates much lower heterogeneity. These observations of lateral heterogeneity are consistent with the conclusion that SAMs in nanografting regions exhibit near molecular-level mixing[23] but reveal phase segregation at the nanoscale in naturally grown systems. The mechanism associated with these observations will be discussed in a later section.

Nanografting Enables Regulation of Surface Concentration in Disulfide:Thiol Binary SAMs. In addition to regulating the local domain arrangement and surface roughness, we found that the surface concentration (*i.e.*, the coverage of alkanethiol in the nanografted binary SAMs) decreases as the nanoshaving speed increases. The surface coverage of the SC_{18} domains in the nanografted

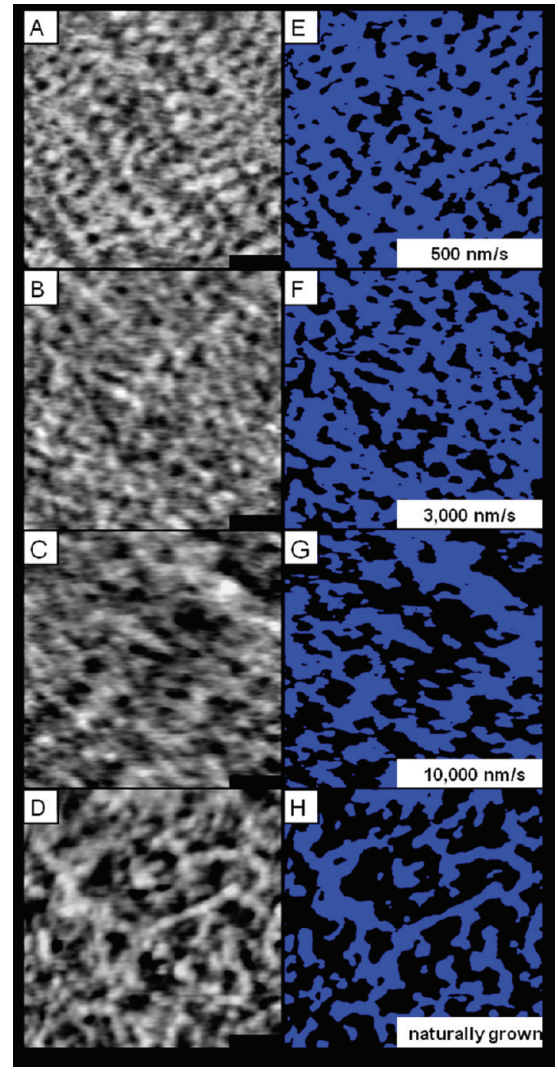

Figure 6. Comparison of the surface coverage of SC_{18} domains in SSC_{11}:SC_{18} binary SAMs nanografted at three shaving speeds: 500, 3000, and 10 000 nm/s and natural growth, from top to bottom. (A−C) High-resolution AFM reveals the local structure of nanografted SAMs formed by shaving speed of (A) 500 nm/s, (B) 3000 nm/s, and (C) 10 000 nm/s. (D) High-resolution AFM reveals the local structure of the naturally grown SAMs. (E−H) Masks show the SC_{18} domains regions of images (A−D), respectively. Scale bars = 20 nm.

SSC_{11}:SC_{18} binary SAMs formed by different nanoshaving speeds is compared in Figure 6. High-resolution AFM images in Figure 6A−C display the local structure of nanografted SSC_{11}:SC_{18} binary SAMs produced at 500, 3000, and 10 000 nm/s, respectively. Figure 6D shows a naturally grown SSC_{11}:SC_{18} binary SAM. The surface coverage of the SC_{18} domains of the nanografted and naturally grown SAMs calculated from the high-resolution images is shown in Figure 6E−H. The surface coverage quantification is described in the Materials and Methods section. At a nanoshaving speed of 500 nm/s, the surface coverage of the SC_{18} is 79 ± 6% (Figure 6E). The SC_{18} domains occupy 65 ± 4% of surface at a higher speed of 3000 nm/s (Figure 6F). When the shaving speed is increased further to 10 000 nm/s, the

TABLE I. Surface Coverage of SC_{18} Domains and Height Difference between Single-Component SC_{18} SAMs and SC_{18} Domains in the Binary SAMs

binary SAMs	surface coverage of SC_{18} domains (%)	height difference between the single-component SC_{18} and the SC_{18} domains of the binary SAMs (nm)
SSC_{11}:SC_{18}		
natural growth	42 ± 3	0.46 ± 0.05
nanografted at 10000 nm/s	51 ± 2	0.36 ± 0.05
nanografted at 3000 nm/s	65 ± 4	0.26 ± 0.05
nanografted at 500 nm/s	79 ± 6	0.14 ± 0.05
$SSC_{10}CHO$:SC_{18}		
natural growth	50 ± 2	0.45 ± 0.05
nanografted at 10000 nm/s	53 ± 3	0.30 ± 0.05
nanografted at 3000 nm/s	60 ± 5	0.20 ± 0.05
nanografted at 500 nm/s	75 ± 2	0.10 ± 0.05

coverage decreases to 51 ± 2% (Figure 6G), which approaches the surface coverage of naturally grown SAMs, 42 ± 3% (Figure 6H). By simply increasing the nanoshaving speed from 500 to 10 000 nm/s, we can decrease the surface coverage of SC_{18} domains by almost 30%.

Assuming the heterogeneity remains constant, a decrease in the apparent heights is anticipated with decreasing SC_{18}. Using single-component SC_{18} SAM as a reference, we can quantify the heights of the nanografted SAMs by nanografting a region of pure SAM nearby, following our previously reported protocols.[39] The quantification of the height difference between the nanografted binary SAMs with respect to the single-component SC_{18} SAM is also described in the Materials and Methods section. At 500 nm/s, the SC_{18} domains are only 0.14 ± 0.05 nm lower than the reference SC_{18} SAM. The nanografted region fell to 0.26 ± 0.05 nm below pure SC_{18} SAM when the shaving speed increases to 3000 nm/s and finally down to 0.36 ± 0.05 nm at a shaving speed of 10 000 nm/s. This trend is consistent with the change in surface composition (*i.e.*, decrease of SC_{18}). As discussed in the previous section, the lateral heterogeneity increases with increasing shaving speed. Therefore, one would expect an opposite trend in terms of apparent height. The decreasing of apparent height with shaving speed indicates that the change in surface composition is significant.

The quantification of surface coverage of the SC_{18} domain and height difference with respect to the SC_{18} SAM of nanografted SAMs is summarized in Table I. The regulation of surface composition is also achieved in a dialkyl disulfide and alkanethiol binary system with aldehyde termini, $SSC_{10}CHO$:SC_{18} binary systems. By increasing the nanoshaving speed from 500 to 10 000 nm/s, the surface coverage of SC_{18} domains decreases from 75 ± 2 to 53 ± 3%.

The finding of regulating surface coverage by altering nanoshaving speed is unique to dialkyl disulfide:

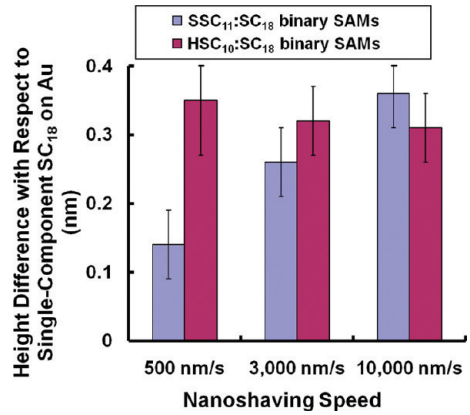

Figure 7. Height differences between a pure SC_{18} SAM and the SC_{18} domains in nanografted binary SAMs of SSC_{11}:SC_{18} (blue bars) and SC_{10}:SC_{18} (purple bars). Binary SAMs were produced at shaving speeds of 500, 3000, and 10 000 nm/s, respectively, from left to right.

alkanethiol binary SAMs when compared to alkanethiol binary SAMs, as seen in Figure 7. Figure 7 illustrates this by plotting nanoshaving speed *versus* the height difference between a single-component SC_{18} SAM and nanografted binary SAMs of SSC_{11}:SC_{18} as well as SC_{10}:SC_{18} at various shaving speeds. The height difference between the nanografted SSC_{11}:SC_{18} binary SAMs and single-component SC_{18} SAM is shown by the blue bars in Figure 7. As the nanoshaving speed increases, the apparent height of SSC_{11}:SC_{18} binary SAMs decreases (*i.e.*, the difference between SC_{18} and binary SAMs apparent height increases), while their alkanethiol counterparts remain relatively the same. In other words, there are more SC_{18} molecules in the binary SAM at slower shaving speeds than at faster shaving speeds. This trend is not observed for the alkanethiol binary SAMs.[23] The height difference of nanografted SC_{10}:SC_{18} binary SAMs and single-component SC_{18} SAMs is shown as the purple bars in Figure 7. The measured height difference remains relatively constant (~0.32 nm), and thus the surface coverage of each component in alkanethiol binary SAMs is not altered by changing nanoshaving speeds.

Spatial Confinement Is Responsible for the Observed Structural Differences. For the naturally grown dialkyl disulfide and alkanethiol binary SAMs, interconnected chains of small alkanethiol domains are observed. The final surface structure represents the trade-off between kinetics and thermodynamics of the SAM formation, which is driven by the interplay between the collision probabilities and lateral mobilities of the alkanethiol and disulfide molecules. The alkanethiol molecules have a slightly larger collision probability and a higher initial lateral mobility when compared to the disulfide molecules. In addition, the intermolecular interaction among SC_{18} molecules is also stronger than SC_{18}−SC_{11} interactions. As a result, SC_{18} molecules form domains, inlaid in SC_{11} areas. In nanografting, especially at slower speed (*e.g.*, 500 nm/s), as shown in Figure 8A, self-assembly follows

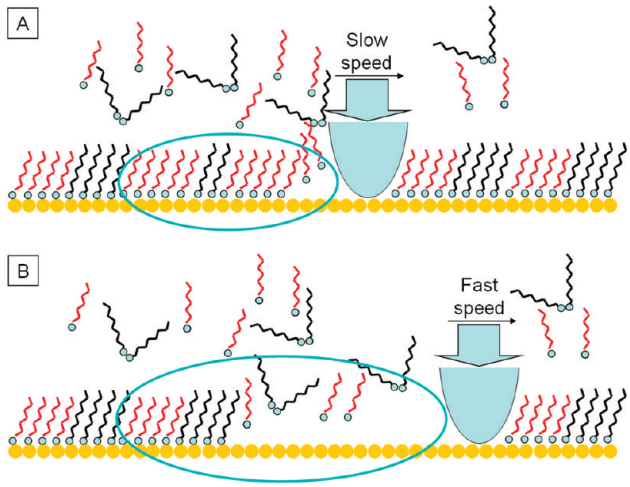

Figure 8. Proposed mechanism to reveal the different adsorption for disulfide and thiol molecules during nanografting under slow and fast shaving speeds. The nanografted regions are highlighted by the blue ellipse. (A) At slow shaving speeds, disulfide molecules have difficulty reaching the Au area due to larger stereohindrance. The attachment probability of disulfide molecules increases with the larger opening above the Au area, thus its coverage may be regulated by the shaving speed. For instance, nanografted SAMs produced by slow shaving speeds have higher coverage of thiol molecules. (B) At fast shaving speeds, newly exposed Au area is no longer spatially confined, and at such, the adsorption of the disulfide and alkanethiol molecules is similar to that in natural growth conditions.

a different pathway due to spatial confinement.[23,40,41] During shaving, the opening above the freshly exposed Au is small and confined by the AFM probe and surrounding SAM. Adsorption of both SC_{18} and SSC_{11} is dictated by the collision; that is, the product is mostly driven by reaction kinetics. Therefore, the resulting structure is more homogeneous. This trend is similar to the pure and mixed alkanethiol SAMs reported previously.[23,40,41]

The unique observation of surface compositional changes can also be explained by spatial confinement effect. Figure 8A and B illustrates the two extreme scenarios at slow and fast shaving speeds, respectively. At slow shaving speeds (*e.g.*, 500 nm/s), the opening above the freshly exposed Au is small and thus surface reaction is confined spatially. The adsorption of alkanethiol molecules (diameter (D) = 0.5 nm in an all-trans conformation) is kinetically favored over dialkyl disulfide molecules ($D > 1.0$ nm assuming all-trans and with the smallest diameter).[42] The dialkyl disulfide molecules have a large cross section compared to the alkanethiol molecules because of the −S−S− functionality and two alkyl chains.[20,42] As a result, the alkanethiol molecules can reach the Au surface more frequently than the dialkyl disulfide molecules. Increasing the nanoshaving speed reduces such difference in occlusion probably with spatial confinement at shaving speeds beyond a threshold, and the space between the tip and adjacent molecules is large and no obvious spatial confinement is observed (blue ellipse). As a result, the self-assembly of the alkanethiol and dialkyl disulfide molecules is unconstrained, and the surface coverage closely resembles that of a naturally grown SAM.

CONCLUSIONS

Nanografting enables the regulation of local structures among binary SAMs of dialkyl disulfide and alkanethiol, including their domain size, domain arrangement, and surface concentration. Intrinsically, naturally grown binary SAMs of dialkyl disulfide:alkanethiol exhibit more complex structures than their alkanethiol counterparts. Nanosized semiellipsoidal domains assemble into large irregular shaped groups. In contrast, most domains of alkanethiol binary SAMs are semiellipsoidal in shape and dispersed almost randomly within the layer. The arrangements of domains may be regulated by altering the shaving speed. At 500 nm/s or slower, small domains of individual components are formed with relatively homogeneous morphology and random dispersion. Increasing shaving speeds does not alter domain size significantly but leads to different domain arrangement, such as a one-dimensional necklace of domains. Beyond a threshold speed of 10 000 nm/s, the local structures exhibit similarity to naturally grown ones. This ability of structural regulation is also demonstrated using non-methyl termini such as aldehyde-terminated disulfide.

In addition to domain arrangement, the surface concentration of dialkyl disulfide and alkanethiol can also be regulated by nanografting. In the systems presented in this investigation, nanografting enables regulation of surface concentration by ~30%. The regulation of surface composition is unique to the inclusion of S−S components. This observation can be rationalized by the mechanism of spatially confined self-assembly. During nanografting, the Au surface is exposed to the mixed thiol solution above. The adsorption of the dialkyl disulfide molecules, which carry larger volume and diameter, encounters stereohindrance at slow speed (*i.e.*, small transient opening) and thus resulted in lower surface composition. Increasing shaving speed facilitates the adsorption of the dialkyl disulfide, toward the naturally grown probabilities. This type of regulation of adsorption is not observed in alkanethiol binary SAMs as those molecules exhibit similar conformation and diameters. Our previous studies demonstrated the spatial confinement nature of self-assembly during nanografting.[43] In the case of single-component reactant, spatial confinement resulted in faster kinetics in adsorption.[43] Using mixed thiols, spatial confinement manifested into regulation of lateral heterogeneity.[23] This investigation revealed another impact of the spatial confinement: by selecting molecules with larger diameters, such as disulfides, both local structures and surface concen-

tration can be regulated using nanografting. Work is in progress to improve the resolution so that molecular level information may be attained. The resulting SAMs can be used to study the protein adhesion behavior, as well as to explore the potential to regulate the local structure and phase of ternary SAMs. This investigation is of generic importance in enhancing our knowledge of local structures of mixed SAMs containing disulfide, and the regulation of local structure is important to surface chemical and biological properties, such as protein immobilization.

MATERIALS AND METHODS

Materials. Hexanethiol, decanethiol, and octadecanethiol (referred to as SC_6, SC_{10}, and SC_{18}, respectively) with purities of 96% were purchased from Sigma Aldrich (St. Louis, MO) and used without further purification. Diundecyl disulfide (referred to as SSC_{11}) with a purity of 98% was purchased from Aldrich and used without further purification. 11-Mercapto-1-undecanal disulfide (referred to as $SSC_{10}CHO$) was purchased from ProChimia (Gdansk, Poland) and used without further purification. Ethanol with a purity of 99.99% was purchased from Gold Shield Chemical Co. (Hayward, CA) and used as the solvent for the mixed alkanethiol solutions. Hexane with a purity of 98.5% was purchased from Sigma Aldrich.

Preparation of Natural Growth Binary SAMs. Preparation of Au substrates followed previous work.[23] Au with a purity of 99.999% was purchased from Alfa Aesar (Ward Hill, MA) and deposited in a high-vacuum evaporator (Denton Vacuum, model DV502-A, Moorestown, NJ) at a base pressure below 2×10^{-6} Torr onto freshly cleaved mica substrates (clear ruby muscovite, Mica New York Corp., New York). The mica was preheated to 350 °C prior to deposition by two quartz lamps mounted behind the mica to enhance the formation of terraced Au(111) domains. Typical evaporation rates were 3 Å/s, and the thickness of the Au films ranged from 1500 to 2000 Å. After evaporation, the Au thin films were annealed at 365 °C under vacuum for 30 min and allowed to cool to room temperature. Immediately after removal from the vacuum chamber, the Au substrates were annealed in a H_2 flame for 2 min in order to produce large terraces ($\geq$10 000 nm^2). The substrates cooled to room temperature in minutes and then were immersed into the premixed dialkyl disulfide and alkanethiol solutions (all ethanol based, 0.02 mM SSC_{11}:SC_{18} = 5:3 or 0.02 mM $SSC_{10}CHO$:SC_{18} = 5:3) for over 20 h. Our previous study on alkanethiol mixed SAMs of SC_{10}:SC_{18} = 5:3 indicated that this solution condition yielded almost equal surface coverage of the two components with characteristic domain morphologies in naturally grown SAMs.[23] This surface structure provides a good starting point for systematic investigations. Therefore, the same ratio of 5:3 was used for SSC_{11}:SC_{18} to form SAMs, which serves as an internal reference for comparing structures with nanografted SAMs. The substrates were rinsed sequentially with ethanol, hexane, and ethanol prior to characterization by AFM.

Atomic Force Microscopy for Imaging and Nanografting. The AFM utilized is a home-constructed, deflection-type scanning head that exhibits high mechanical stability.[23,43] The scanner was controlled by an AFM 100 preamplifier and SPM 100 electronics (RHK Technology, Inc. Troy, MI). The AFM scanner was calibrated laterally *via* the periodicity of a mica(0001) surface (0.518 nm) and vertically using the single atomic step of a Au(111) surface (0.235 nm). Sharpened Si microlevers (model MSNL, Veeco Metrology Group, Santa Barbara, CA) with force constants of 0.1 N/m or Si microlevers (model HYDRA2R-50NG, AppNano, Santa Clara, CA) with force constants of 0.084 N/m were used for imaging. Images were acquired using contact mode in mixed or pure thiol and/or disulfide ethanol solutions. The image rate was 1 Hz, and typical image forces ranged from 2 to 3 nN.

Nanografting is an AFM-based fabrication method developed and reported by the Liu group.[43−45] Briefly, for the present work, a SAM prepared by natural growth serves as a matrix, which is immersed in a solution containing the desired replacement molecules. The matrix is imaged by the AFM tip under a low load (2−3 nN). Once the fabrication location is determined, the load is increased to above the displacement threshold (20 nN) of the adsorbed thiolated molecules. During the scanning, the matrix molecules are removed and replaced by thiols in solution as the AFM tip shaves through the matrix monolayer.[23,40,43−45]

Determining the Local Structure and Surface Coverage. The local structure of the binary SAMs was visualized with high-resolution AFM images, from which the lateral heterogeneity and surface coverage were determined. For each high-resolution image, the lateral size and apparent height of the SC_{18} domains in the binary SAMs were measured from at least 15 cursor profiles across characteristic domains. The width of the SC_{18} domains was determined at the full width at half-maximum of the peaks from the cursor profiles. For each binary SAM, at least two images were analyzed, and their averages and standard deviations were extracted from the cumulative analysis.

The difference in apparent height between the naturally grown and the nanografted regions was measured from the peak of the bright domains in the naturally grown regions to that in nanografted regions, assuring that both regions were on the same Au(111) terrace. At least 5 cursor profiles for each image were taken. Our previously established method was used to quantify the true height of the domains within mixed SAMs: by nanografting a single-component SC_{18} within a naturally grown region of interests.[39] The SC_{18} SAM's height is well-known (2.23 nm) and served as an excellent internal standard.

The surface concentration (*i.e.*, the coverage of each component) was calculated from selected regions using a custom script written in Matlab (version 7.6.0, The MathWorks. Inc., Natick, MA) as described previously.[46,47] For each AFM image, the surface coverage of the bright domains (θ_{bright}) was determined by counting the number of pixels above the domain height difference between the bright and gray domains (P_{bright}) and dividing by the total number of pixels in the image (P_{total}). In other words, the surface coverage of the bright domains is $\theta_{bright} = P_{bright}/P_{total}$. The threshold value for the masks was calculated using the full width at half-height between the bright and gray domains for at least 10 cursor profiles per AFM image. Defects in the substrate, imaged as dark domains, were excluded.

Acknowledgment. We thank Drs. Jie-ren Li, Bo Gao, Jessica Koehne, Lifang Shi, and Christopher Fleming for many helpful discussions. This work was supported by NSF (CHE-0809977) and University of California, Davis.

REFERENCES AND NOTES

1. Bain, C. D.; Evall, J.; Whitesides, G. M. Formation of Monolayers by the Coadsorption of Thiols on Gold: Variation in the Head Group, Tail Group, and Solvent. *J. Am. Chem. Soc.* **1989**, *111*, 7155–7164.
2. Bain, C. D.; Whitesides, G. M. Formation of Monolayers by the Coadsorption of Thiols on Gold: Variation in the Length of the Alkyl Chain. *J. Am. Chem. Soc.* **1989**, *111*, 7164–7175.
3. Imabayashi, S.; Gon, N.; Sasaki, T.; Hobara, D.; Kakiuchi, T. Effect of Nanometer-Scale Phase Separation on Wetting of Binary Self-Assembled Thiol Monolayers on Au(111). *Langmuir* **1998**, *14*, 2348–2351.
4. Fan, F. R. F.; Yao, Y. X.; Cai, L. T.; Cheng, L.; Tour, J. M.; Bard,

A. J. Structure-Dependent Charge Transport and Storage in Self-Assembled Monolayers of Compounds of Interest in Molecular Electronics: Effects of Tip Material, Headgroup, and Surface Concentration. *J. Am. Chem. Soc.* **2004**, *126*, 4035–4042.
5. Choi, S. H.; Lee, J. W.; Sim, S. J. Enhanced Performance of a Surface Plasmon Resonance Immunosensor for Detecting Ab-GAD Antibody Based on the Modified Self-Assembled Monolayers. *Biosens. Bioelectron.* **2005**, *21*, 378–383.
6. Kwon, Y.; Han, Z. Z.; Karatan, E.; Mrksich, M.; Kay, B. K. Antibody Arrays Prepared by Cutinase-Mediated Immobilization on Self-Assembled Monolayers. *Anal. Chem.* **2004**, *76*, 5713–5720.
7. Liu, M. Z.; Liu, G. Y. Hybridization with Nanostructures of Single-Stranded DNA. *Langmuir* **2005**, *21*, 1972–1978.
8. Balamurugan, S.; Ista, L. K.; Yan, J.; Lopez, G. P.; Fick, J.; Himmelhaus, M.; Grunze, M. Reversible Protein Adsorption and Bioadhesion on Monolayers Terminated with Mixtures of Oligo(ethylene glycol) and Methyl Groups. *J. Am. Chem. Soc.* **2005**, *127*, 14548–14549.
9. Murphy, W. L.; Mercurius, K. O.; Koide, S.; Mrksich, M. Substrates for Cell Adhesion Prepared *via* Active Site-Directed Immobilization of a Protein Domain. *Langmuir* **2004**, *20*, 1026–1030.
10. Li, L. Y.; Chen, S. F.; Jiang, S. Y. Nanoscale Frictional Properties of Mixed Alkanethiol Self-Assembled Monolayers on Au(111) by Scanning Force Microscopy: Humidity Effect. *Langmuir* **2003**, *19*, 666–671.
11. Price, W. J.; Kuo, P. K.; Lee, T. R.; Colorado, R.; Ying, Z. C.; Liu, G. Y. Probing the Local Structure and Mechanical Response of Nanostructures Using Force Modulation and Nanofabrication. *Langmuir* **2005**, *21*, 8422–8428.
12. Price, W. J.; Leigh, S. A.; Hsu, S. M.; Patten, T. E.; Liu, G. Y. Measuring the Size Dependence of Young's Modulus Using Force Modulation Atomic Force Microscopy. *J. Phys. Chem. A* **2006**, *110*, 1382–1388.
13. Lahiri, J.; Isaacs, L.; Grzybowski, B.; Carbeck, J. D.; Whitesides, G. M. Biospecific Binding of Carbonic Anhydrase to Mixed SAMs Presenting Benzenesulfonamide Ligands: A Model System for Studying Lateral Steric Effects. *Langmuir* **1999**, *15*, 7186–7198.
14. Tan, Y. H.; Liu, M.; Nolting, B.; Go, J. G.; Gervay-Hague, J.; Liu, G. Y. A Nanoengineering Approach for Investigation and Regulation of Protein Immobilization. *ACS Nano* **2008**, *2*, 2374–2384.
15. Houseman, B. T.; Gawalt, E. S.; Mrksich, M. Maleimide-Functionalized Self-Assembled Monolayers for the Preparation of Peptide and Carbohydrate Biochips. *Langmuir* **2003**, *19*, 1522–1531.
16. Nuzzo, R. G.; Allara, D. L. Adsorption of Bifunctional Organic Disulfide on Gold Surfaces. *J. Am. Chem. Soc.* **1983**, *105*, 4481–4483.
17. Bateman, L.; Cunneen, J. I.; Ford, J. Oxidation of Organic Sulphides 0.8. Autoxidation of Thiacyclohexane, 2-Ethyl-2-methyl-5-isopropylthiacyclopentane, and Thacyclohex-3-Ene. *J. Chem. Soc.* **1957**, 1539–1544.
18. Lee, J. E.; Didier, D. N.; Lockett, M. R.; Scalf, M.; Greene, A. S.; Olivier, M.; Smith, L. M. Characterization of Vascular Endothelial Growth Factor Receptors on the Endothelial Cell Surface during Hypoxia Using Whole Cell Binding Arrays. *Anal. Biochem.* **2007**, *369*, 241–247.
19. Haussling, L.; Michel, B.; Ringsdorf, H.; Rohrer, H. Direct Observation of Streptavidin Specifically Adsorbed on Biotin-Functionalized Self-Assembled Monolayers with the Scanning Tunneling Microscope. *Angew. Chem., Int. Ed. Engl.* **1991**, *30*, 569–572.
20. Biebuyck, H. A.; Bian, C. D.; Whitesides, G. M. Comparison of Organic Monolayers on Polycrystalline Gold Spontaneously Assembled from Solutions Containing Dialkyl Disulfides or Alkanethiols. *Langmuir* **1994**, *10*, 1825–1831.
21. Strong, L.; Whitesides, G. M. Structures of Self-Assembled Monolayer Films of Organosulfur Compounds Adsorbed on Gold Single Crystals: Electron Diffraction Studies. *Langmuir* **1988**, *4*, 546–558.
22. Chen, S. F.; Li, L. Y.; Boozer, C. L.; Jiang, S. Y. Controlled Chemical and Structural Properties of Mixed Self-Assembled Monolayers by Coadsorption of Symmetric and Asymmetric Disulfides on Au(111). *J. Phys. Chem. B* **2001**, *105*, 2975–2980.
23. Yu, J. J.; Tan, Y. H.; Li, X.; Kuo, P. K.; Liu, G. Y. A Nanoengineering Approach To Regulate the Lateral Heterogeneity of Self-Assembled Monolayers. *J. Am. Chem. Soc.* **2006**, *128*, 11574–11581.
24. Wadu-Mesthrige, K.; Amro, N. A.; Garno, J. C.; Xu, S.; Liu, G. Y. Fabrication of Nanometer-Sized Protein Patterns Using Atomic Force Microscopy and Selective Immobilization. *Biophys. J.* **2001**, *80*, 1891–1899.
25. Liu, G. Y.; Amro, N. A. Positioning Protein Molecules on Surfaces: A Nanoengineering Approach to Supramolecular Chemistry. *Proc. Natl. Acad. Sci. U.S.A.* **2002**, *99*, 5165–5170.
26. Poirier, G. E. Characterization of Organosulfur Molecular Monolayers on Au(111) Using Scanning Tunneling Microscopy. *Chem. Rev.* **1997**, *97*, 1117–1127.
27. Poirier, G. E. Mechanism of Formation of Au Vacancy Islands in Alkanethiol Monolayers on Au(111). *Langmuir* **1997**, *13*, 2019–2026.
28. Qian, Y. L.; Yang, G. H.; Yu, J. J.; Jung, T. A.; Liu, G. Y. Structures of Annealed Decanethiol Self-Assembled Monolayers on Au(111): An Ultrahigh Vacuum Scanning Tunneling Microscopy Study. *Langmuir* **2003**, *19*, 6056–6065.
29. Hobara, D.; Ota, M.; Imabayashi, S.; Niki, K.; Kakiuchi, T. Phase Separation of Binary Self-Assembled Thiol Monolayers Composed of 1-Hexadecanethiol and 3-Mercaptopropionic Acid on Au(111) Studied by Scanning Tunneling Microscopy and Cyclic Voltammetry. *J. Electroanal. Chem.* **1998**, *444*, 113–119.
30. Kakiuchi, T.; Iida, M.; Gon, N.; Hobara, D.; Imabayashi, S.; Niki, K. Miscibility of Adsorbed 1-Undecanethiol and 11-Mercaptoundecanoic Acid Species in Binary Self-Assembled Monolayers on Au(111). *Langmuir* **2001**, *17*, 1599–1603.
31. Klein, H.; Battaglini, N.; Bellini, B.; Dumas, P. STM of Mixed Alkylthiol Self-Assembled Monolayers on Au(111). *Mater. Sci. Eng., C* **2002**, *19*, 279–283.
32. Sawaguchi, T.; Sato, Y.; Mizutani, F. *In Situ* STM Imaging of Individual Molecules in Two-Component Self-Assembled Monolayers of 3-Mercaptopropionic Acid and 1-Decanethiol on Au(111). *J. Electroanal. Chem.* **2001**, *496*, 50–60.
33. Riposan, A.; Li, Y.; Tan, Y. H.; Galli, G.; Liu, G. Y. Structural Characterization of Aldehyde-Terminated Self-Assembled Monolayers. *J. Phys. Chem. A* **2007**, *111*, 12727–12739.
34. Burnham, N. A.; Dominguez, D. D.; Mowery, R. L.; Colton, R. J. Probing the Surface Forces of Monolayer Films with an Atomic-Force Microscope. *Phys. Rev. Lett.* **1990**, *64*, 1931–1934.
35. Mate, C. M.; McClelland, G. M.; Erlandsson, R.; Chiang, S. Atomic-Scale Friction of a Tungsten Tip on a Graphite Surface. *Phys. Rev. Lett.* **1987**, *59*, 1942–1945.
36. Noy, A.; Frisbie, C. D.; Rozsnyai, L. F.; Wrighton, M. S.; Lieber, C. M. Chemical Force Microscopy-Exploting Chemically-Modified Ttips to Quantify Adhesion, Friction, and Functional-Group Distributions in Molecular Assemblies. *J. Am. Chem. Soc.* **1995**, *117*, 7943–7951.
37. Ogletree, D. F.; Carpick, R. W.; Salmeron, M. Calibration of Frictional Forces in Atomic Force Microscopy. *Rev. Sci. Instrum.* **1996**, *67*, 3298–3306.
38. Overney, R. M.; Meyer, E.; Frommer, J.; Brodbeck, D.; Luthi, R.; Howald, L.; Guntherodt, H. J.; Fujihira, M.; Takano, H.; Gotoh, Y. Friction Measurements on Phase-Separated Thin-Films with a Modified Atomic Force Microscope. *Nature* **1992**, *359*, 133–135.
39. Liu, M.; Amro, N. A.; Liu, G. Y. Nanografting for Surface Physical Chemistry. *Annu. Rev. Phys. Chem.* **2008**, *59*, 367–386.

40. Xu, S.; Laibinis, P. E.; Liu, G. Y. Accelerating the Kinetics of Thiol Self-Assembly on Gold: A Spatial Confinement Effect. *J. Am. Chem. Soc.* **1998**, *120*, 9356–9361.
41. Ryu, S.; Schatz, G. C. Nanografting: Modeling and Simulation. *J. Am. Chem. Soc.* **2006**, *128*, 11563–11573.
42. Dixon, D. A.; Zeroka, D.; Wendoloski, J. J.; Wasserman, Z. R. The Molecular Structure of H_2S_2, and Barriers to Internal Rotation. *J. Phys. Chem.* **1985**, *89*, 5334–5336.
43. Xu, S.; Liu, G. Y. Nanometer-Scale Fabrication by Simultaneous Nanoshaving and Molecular Self-Assembly. *Langmuir* **1997**, *13*, 127–129.
44. Xu, S.; Liu, G. Y. Fabrication of Nanometer Scale Patterns within Self-Assembled Monolayers Using Nanografting. *Scanning* **1999**, *21*, 71.
45. Xu, S.; Miller, S.; Laibinis, P. E.; Liu, G. Y. Fabrication of Nanometer Scale Patterns within Self-Assembled Monolayers by Nanografting. *Langmuir* **1999**, *15*, 7244–7251.
46. Dameron, A. A.; Hampton, J. R.; Smith, R. K.; Mullen, T. J.; Gillmor, S. D.; Weiss, P. S. Microdisplacement Printing. *Nano Lett.* **2005**, *5*, 1834–1837.
47. Mullen, T. J.; Dameron, A. A.; Saavedra, H. M.; Williams, M. E.; Weiss, P. S. Dynamics of Solution Displacement in 1-Adamantanethiolate Self-Assembled Monolayers. *J. Phys. Chem. C* **2007**, *111*, 6740–6746.